metals

MDPI

Article

Influence of Intergranular Mechanical Interactions on Orientation Stabilities during Rolling of Pure Aluminum

Weimin Mao

State Key Laboratory of advanced Metals and Materials, University of Science and Technology Beijing, Xue-Yuan Road 30, Beijing 100083, China; wmmao@ustb.edu.cn; Tel.: +86-10-6233-2300

Received: 22 February 2019; Accepted: 23 April 2019; Published: 25 April 2019

Abstract: Taylor strain principles are widely accepted in current predominant crystallographic deformation theories and models for reaching the necessary stress and strain equilibria in polycrystalline metals. However, to date, these principles have obtained neither extensive experimental support nor sufficient theoretical explanation and understanding. Therefore, the validity and necessity of Taylor strain principles is questionable. The present work attempts to calculate the elastic energy of grains and their orientation stabilities after deformation, whereas the stress and strain equilibria are reached naturally, simply and reasonably based on the proposed reaction stress (RS) model without strain prescription. The RS model is modified by integrating normal RS in the transverse direction of rolling sheets into the model. The work hardening effect, which is represented by an effective dislocation distance, is connected with the engineering strength level of metals. Crystallographic rolling texture development in roughly elastic isotropic pure aluminum is simulated based on the modified RS model, whereas orientation positions and peak densities of main texture components, i.e., brass, copper and S texture, can be predicted accurately. RS σ_{12} commonly accumulates to a high level and features a strong influence on texture formation, whereas RS σ_{23} and σ_{31} hardly accumulate and can only promote random texture. Cube orientations can obtain certain stability under the effects of RSs including σ_{22}. A portion of elastic strain energy remains around the grains. This phenomenon is orientation-dependent and connected to RSs during deformation. The grain stability induced by elastic strain energy may influence grain behavior in subsequent recovery or recrystallization.

Keywords: intergranular interaction; reaction stress; texture simulation; rolling deformation; aluminum

1. Introduction

In general, stress and strain equilibria are maintained during and after the plastic deformation of polycrystalline metals. Equilibria should occur in forms in which stress and strain are fluctuant when penetrating the polycrystalline body. Fluctuations may depend on grain size and shape, locations within grains or around the grain boundary areas, grain orientations and misorientations between grains and the strength levels of metals. Fluctuations of stresses and strains after plastic deformation result from intergranular mechanical interactions during the same process. Equilibria are reached in the current crystallographic deformation theories and models predominantly based on the Taylor strain principles [1]; these models include the viscoplastic self-consistent (VPSC) model [2], the advanced Lamel model [3] and the grain-interaction model [4], which prescribes in advance that the strain tensor of grains or grain clusters is basically identical to the macroscopic strain tensor during plastic deformation; this strain tensor prevails everywhere but shows minimal fluctuation

inside polycrystalline aggregates. The Taylor principles have not obtained sufficient theoretical explanation and understanding. However, experimental observations indicated that plastic strain tensors of individual grains in the same deformation aggregate often differ from each other and from the macroscopic strain tensor [5]. Meanwhile, the most widely used VPSC model based on the prescribed Taylor principles often fails to correctly predict certain crystallographic textures [6–10]. Therefore, whether the Taylor principles are acceptable or necessary remains questionable [11].

A reaction stress (RS) model was proposed [12,13] based on intergranular mechanical interactions during deformation. The model attempts to avoid any prescription of stress or strain tensors in advance, calculates the intergranular RSs stepwise during deformation and traces the necessary multiple slips under the combination of external and intergranular stresses in a natural, simple, reasonable, easily understandable and acceptable manner. In the present work, the RS model was improved in a way that all possible RSs are integrated and can be controlled separately. Furthermore, an effective dislocation distance is introduced according to the strength level of deformation metals instead of the previously estimated value. Based on the improvements—especially in aluminum, which is approximately an elastic isotropic metal—the model can simulate deformation processes and predict texture formation accurately, possibly facilitating a deep understanding of the deformation behavior of polycrystalline metals and other corresponding behaviors, e.g., recovery behavior in subsequent thermal treatment.

2. Intergranular Mechanical Interactions

Suppose that the plastic deformation of a gray grain (Figure 1a,b) in a polycrystalline sample of interstitial-free steel [13] proceeds first under external rolling stress, whereas a slip system with the maximal Schmid factor is activated (Figure 1b). The plastic strain tensor produced by a tiny slip of the slip system will immediately induce stress and strain incompatibility between the concerned grain and its neighboring grains. The slip must encounter resistance from the neighboring grains first in the form of elastic RSs. The plastic strains produced will be partially reduced in an elastic manner, whereas the neighboring grains must also be strained elastically to a certain extent. Therefore, the incompatible part of the plastic strain produced is relieved by the elastic strains of both the concerned grain and its neighboring grains. Between these grains, stress and strain equilibria are reached elastically and naturally according to Hooke's law. If these behaviors appear in an elastic isotropic metal, e.g., aluminum, not only the RS values but also the elastic reaction strain values of the grain concerned and its neighboring grains become equal by reaching the stress and strain equilibria.

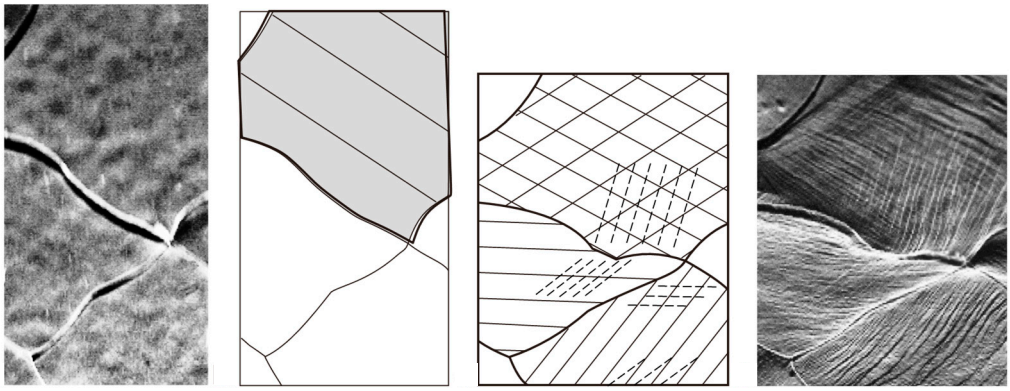

(**a**) (**b**) (**c**) (**d**)

Figure 1. Grain structure evolution before and after compression of an interstitial-free steel sample, Reproduced with permission from [13], Elsevier, 2016; analysis of intergranular mechanical interaction and corresponding stress and strain equilibria. (**a**) Grains before deformation; (**b**) stress and strain incompatibility induced by the first penetrating slip (parallel real lines in gray grain); (**c**) multi-slips of penetrating (parallel real lines) and nonpenetrating local slips (parallel dashed lines) under the combination of external stress and internal reaction stresses (RSs); (**d**) experimental observation of penetrating and nonpenetrating local slips.

The stress tensor $[\sigma_{ij}]$ bore by the concerned grain after the first slip becomes the combination of external stress and RS [12,13] as follows:

$$\left[\sigma_{ij}\right] = \sigma_y \begin{bmatrix} \frac{1}{2} & 0 & 0 \\ 0 & 0 & 0 \\ 0 & 0 & -\frac{1}{2} \end{bmatrix} - \sigma_y \begin{bmatrix} -\mu\varepsilon_{22}\frac{d}{b} & \mu\varepsilon_{12}\frac{d}{b} & \mu\varepsilon_{13}\frac{d}{b} \\ \mu\varepsilon_{21}\frac{d}{b} & \mu\varepsilon_{22}\frac{d}{b} & \mu\varepsilon_{23}\frac{d}{b} \\ \mu\varepsilon_{31}\frac{d}{b} & \mu\varepsilon_{32}\frac{d}{b} & 0 \end{bmatrix} \quad (1)$$

where the first and second terms refer to the external rolling stress tensor and internal RS tensor, respectively; ε_{ij} denotes the plastic strain produced by the slip [13]; 1, 2 and 3 represent the rolling direction, transverse direction (TD) and normal direction of the rolling sheet, respectively; σ_y indicates the macroscopic flow yield stress during rolling; μ specifies the generalized Schmid factor of the activated slip system; d corresponds to the effective distance between dislocations; b is the length of the Burgers vector. The normal RS in the TD is included in Equation (1) in comparison with the previous formula [13]; thus, all possible RSs are considered. Meanwhile, the effective distance d is used to replace the previously estimated average. The approximate relationship between σ_y and yield shear stress τ_y [14] and the related effective distance d can be expressed according to the Frank-Read theory as follows [14]:

$$\tau_y = \frac{\sigma_y}{2} = \frac{Gb}{d} \text{ or } d = \frac{2Gb}{\sigma_y} \quad (2)$$

where G is the shear modulus. The flow yield stress σ_y before the deformation of an annealed metal, i.e., σ_{y0}, denotes the yield strength and its top limit in an extremely hardened state, e.g., at $\varepsilon_{33} = -4.0$ (98% rolling reduction), can be the tensile strength σ_b. According to the conventional flow stress of most deformation metals, the flow yield stress σ_y for the present simulation can be assumed to develop with a rolling reduction of $\varepsilon_{33} < 0$ as follows:

$$\sigma_y = \sigma_{y0} + \left(\sigma_b - \sigma_{y0}\right) \cdot \sqrt[n]{\frac{-\varepsilon_{33}}{4}} \quad (3)$$

where σ_{y0} = 20 MPa and σ_b = 50 MPa are valid for aluminum and n = 8 is used in the present work to obtain a proper flow stress for the early work hardening rate. The RSs indicated in Equation (1) accumulate with increasing rolling deformation until the Schmid factor of another slip system sufficiently

increases. The new slip system with a high Schmid factor will be instantaneously activated, whereas RSs further accumulate and several RS components might be reduced. The slips can alternatively be followed step by step in multiple ways (Figure 1c, indicated by parallel real lines) under the stress tensor of Equation (1). Any reasonable activation and combination of slip systems requested by the multiple slip can be implemented if the calculation step is sufficient small.

However, the accumulated RSs should feature a limitation and yield point that must not be exceeded. The limitations of deformation stress components $[\sigma_{ij}]_{\text{lim}}$ indicated in Equation (1) [13], including that of the normal RS in the TD, are as follows:

$$\left[\sigma_{ij}\right]_{\text{lim}} = \begin{bmatrix} \sigma_{11} \equiv -\sigma_{33} - \sigma_{22} & |\sigma_{12}| \le \alpha_{12}\sigma_y/2 & |\sigma_{13}| \le \alpha_{31}\sigma_y/2 \\ |\sigma_{21}| \le \alpha_{12}\sigma_y/2 & |\sigma_{22}| \le \alpha_{22}\sigma_y/2 & |\sigma_{23}| \le \alpha_{23}\sigma_y/2 \\ |\sigma_{31}| \le \alpha_{31}\sigma_y/2 & |\sigma_{32}| \le \alpha_{23}\sigma_y/2 & \sigma_{33} \equiv -\sigma_y/2 \end{bmatrix} \quad (4)$$

where α_{ij} represents the effective coefficient of maximal RSs ranging from 0 to 1. $\alpha_{ij} \equiv 0$ means no RS, similar to that of the Sachs model [15], whereas $\alpha_{ij} \equiv 1$ implies that the highest reaction shear stress possible occurs.

Plastic behavior is observed by means of slip traces (Figure 1d) in all grains during deformation. If any of the RSs acting on a concerned grain reaches its upper limit, as shown in Equation (4), certain slip systems in the neighboring grains may be additionally activated on the boundary area in addition to the normal penetrating slips. In this case, the stress and strain equilibria cannot be maintained elastically as discussed above but also by the local plastic behavior around the boundary areas, as induced by several nonpenetrating slips (Figure 1c, indicated by parallel dashed lines) on which shear stress has reached the critical value for activation. The nonpenetrating characteristics of the slips imply that stress and plastic strain in equilibrium run fluctuant from one grain over the boundary to another grain (Figure 1d) and cannot be similar to that predicted by the Taylor principles.

3. Orientation Stabilities during Rolling of Pure Aluminum

Studies have indicated that plastic deformation is conducted by penetrating and nonpenetrating slips, e.g., in polycrystalline aluminum in which the dislocation slip is the only crystallographic deformation mechanism observed. Notably, penetrating slips will change grain orientations regularly, whereas nonpenetrating slips will change orientations randomly, i.e., the former induces deformation texture and the latter induces random texture.

A slip system undergoes shear stress during deformation regardless of the activity state of the slip system. This phenomenon may reduce the necessary RS for additional activations of nonpenetrating slips. Therefore, the upper limits shown in Equation (4) may not be reached when nonpenetrating slips become active, i.e., the effective coefficients α_{ij} are commonly lower than 1, although they should be higher than 0. Thus, the optimum α_{ij} value should be investigated.

The main texture components after the heavy rolling of aluminum commonly include copper texture {90°, 30°, 45°}, brass texture {35°, 45°, 0°/90°} and S texture {55°, 35°, 65°}. Goss texture {0°, 45°, 0°/90°} can remain at low rolling reduction [16]. On the other hand, the Taylor model predicts the Taylor texture {90°, 25°, 45°} [13,16]. All these components, including the cube texture {45°, 0°, 45°}, can be predicted by the RS model if the α_{ij} values are selected properly (Figure 2, sections of orientation distribution functions (ODF)).

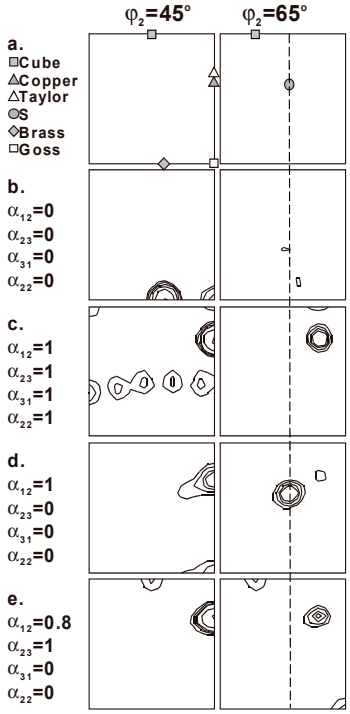

Figure 2. Relationship between the effective coefficient α_{ij} and stabilities of the main rolling texture components in aluminum at 95% rolling reduction simulated by the RS model based on 936 initial random orientations [17]. ($\varepsilon_{33} = -3.0$, i.e., 95% reduction; simulation steps $\Delta\varepsilon_{33} = 0.001$; orientation distribution functions (ODF) $\varphi_2 = 45°$ and $\varphi_2 = 65°$ sections; density levels: 5, 10, 20, 40, 80 and 160). (**a**) Orientation position of texture components; (**b**) stable brass and Goss textures at $\alpha_{12} = \alpha_{23} = \alpha_{31} = \alpha_{22} = 0$; (**c**) stable Taylor texture at $\alpha_{12} = \alpha_{23} = \alpha_{31} = \alpha_{22} = 1$; (**d**) stable S texture at $\alpha_{12} = 1$ and $\alpha_{23} = \alpha_{31} = \alpha_{22} = 0$; (**e**) stable copper and cube textures at $\alpha_{12} = 0.8$, $\alpha_{23} = 1$ and $\alpha_{31} = \alpha_{22} = 0$.

High α_{ij} values mean that high RSs can be accumulated, thus jointly determining the selection of penetrating slips together with external stress and influencing orientation evolutions and texture formation. Low α_{ij} values imply that only low RSs possibly occur, whereas nonpenetrating slips can be induced easily, in which stress and strain equilibria between grains are maintained locally in a plastic manner. In this case, nonpenetrating slips will only induce random evolution of grain orientations and cannot be included directly in the simulation of texture formation in the RS model. This random effect can be represented by introducing a random fraction into the simulated deformation texture of the RS model.

Metal crystals are plastically anisotropic regardless of whether they are elastically isotropic. The activated slip system and the produced strain tensor in a grain are grain orientation-dependent. The maximum RS that can be obtained and the upper limit, i.e., the α_{ij} value of an RS in Equation (4) allowed to induce nonpenetrating slips in neighboring grains, depend not only on the orientation of the concerned grain but also on the orientations of neighboring grains. Infinite possibilities of orientation combinations exist between two neighboring grains and the corresponding α_{ij} values are characterized differently for each possibility. Thus, considering all possibilities will present considerable difficulty and require considerable computation [3,4]. Therefore, the problem should be approached in a statistical manner.

4. Simulation of Normal Rolling Texture in Pure Aluminum

An aluminum ingot with commercial purity (99.9% Al) was forged in three directions with reducing forging reductions (25%, 15%, 10% and 5%), followed by annealing at 500 °C for 10 min [16]. Then, a sample with 8.6 mm thickness and a random initial texture was cut. The sample was cold-rolled

down to reductions of 30%, 50%, 70%, 90% and 95%, while the true strain ε_{33} reached −0.36, −0.7, −1.2, −2.1 and −3.0, respectively. Figure 3a provides the rolling textures in ODF sections, in which the evolution of copper and brass textures in the φ_2 = 45° section and the S texture in theφ_2 = 65° section (Figure 2a) during rolling can be observed.

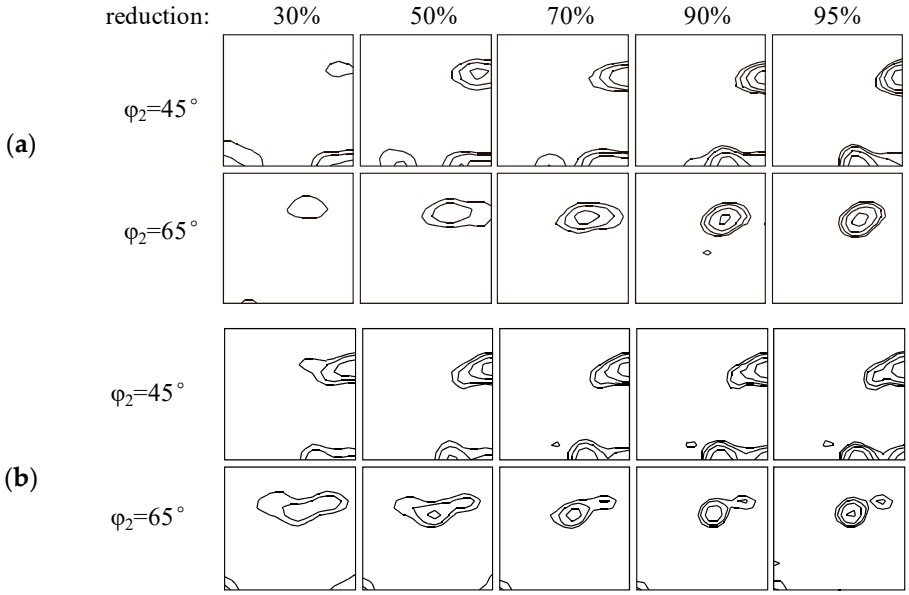

Figure 3. Development of rolling texture in commercial-purity aluminum and corresponding simulation based on the RS model, as observed in ODF φ_2 = 45° andφ_2 = 65° sections (density levels: 2, 4, 8 and 16). (**a**) Experimental texture; (**b**) corresponding texture simulation including 10% random texture (936 initial random orientations; simulation steps $\Delta\varepsilon_{33}$ = 0.001, α_{12} = 0.72, α_{23} = α_{31}= 0, α_{22} = 0.04), based on the RS model.

The α_{ij} values must be determined for simulating the rolling texture based on the RS model and they are influenced by grain orientations and the orientations of neighboring grains. The α_{ij} values may also change during rolling deformation. Nevertheless, the most frequent and common α_{ij} values are obtained from a statistical point of view and the values total α_{12} = 0.72, α_{23} = α_{31} = 0 and α_{22} = 0.04. Figure 3b shows the simulation results, including 10% random texture resulting from the nonpenetrating slips. The ODF density would become too high without the 10% random texture. This outcome is very similar to the experimental observations (Figure 3a) showing the central positions of copper, brass and S textures and their peak densities. The results indicate that the RS model can predict and reproduce the formation of rolling texture in aluminum.

Activated slip systems commonly produce a low normal strain ε_{22} in the TD under external rolling stress (first term of Equation (1)), and a high RS and α_{22} cannot be expected. Low α_{22} also means that normal RS in the TD cannot accumulate to high levels before the corresponding nonpenetrating slips in neighboring grains become active under external loading. Figure 4 schematically demonstrates the three shear strains ε_{ij} ($i \neq j$ refers to Equation (1)) produced by the activation of the slip systems. Qualitatively, strains ε_{23} and ε_{31} and the corresponding RSs should become limited, especially as the ratio of grain thickness to length or width decreases [18]. Strain ε_{12}, by contrast, may cause severe strain incompatibility across the boundary parallel to the sheet plane if the grains have become flat. However, no quantitative calculation was conducted to describe the phenomena, but ε_{23} and ε_{31} appeared without restriction and ε_{12} was restricted to zero according to the Taylor principles [18]. In return, the RS model arrives at a similar conclusion, but it can quantitatively calculate the maximum RS and explain the detailed mechanism by which shear strain is compensated to maintain stress and strain equilibria. High α_{12} (>0.7) means that high σ_{12} can be accumulated and ε_{12} is compensated mainly by the selection of penetrating slips. α_{23} = α_{31} = 0 means that ε_{23} and ε_{31} are compensated

mainly by local nonpenetrating slips around the boundary areas. The textures simulated will disagree visibly with experimental observations (Figure 3a) if different α_{ij} values are used.

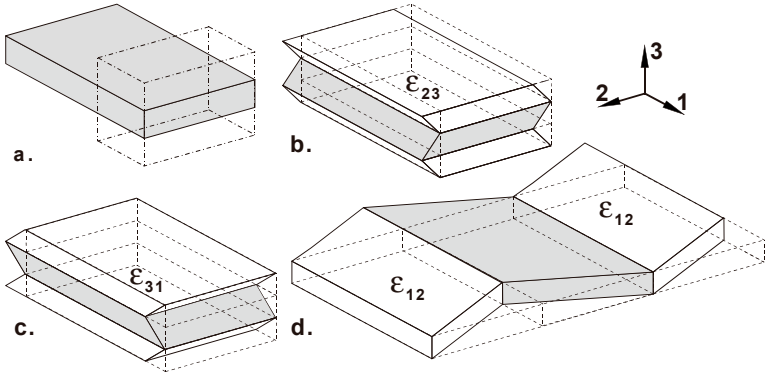

Figure 4. Shear strains ε_{ij} that may be produced in a gray grain during rolling while considering the manner of strain compensation.

Higher α_{ij} means possibly, but not necessarily, higher RSs. The α_{ij} values for texture simulation (Figure 3b) are the same for all grains, since they will encounter similar environments after texture formation at higher rolling reduction. However, the approximation between the actual simulated RSs of individual grains and the limitations $\alpha_{ij}\sigma_y/2$ in Equation (4) depends on the grain orientations.

5. Orientation Dependency of Elastic Strain Energy after Rolling

Elastic stress and strain will be induced if external loading is applied on a polycrystalline metal regardless of plastic behavior. The elastic stress and strain will disappear if external loading is removed and only plastic strain will remain if any plastic strain has appeared. However, the elastic stresses and strains induced by intergranular interactions of individual grains during deformation will also remain. This elastic stress-and-strain condition cannot be relieved by the removal of external loading. Therefore, a part of the elastic energy of different grains remains after plastic deformation in addition to normally stored energy. RSs $\sigma_{33} = 0$ and $\sigma_{11} = -\sigma_{22}$ are valid, whereas the deformation volume remains basically constant by the removal of external loading. The elastic energy W around the boundary area can then be calculated according to the elastic theory and the remaining RS σ_{ij} after deformation of differently oriented grains:

$$W = \frac{1}{2G}\left(\sigma_{12}^2 + \sigma_{23}^2 + \sigma_{31}^2 + \sigma_{22}^2\right) \quad (5)$$

where $G = 26$ GPa is valid for aluminum. The orientations based on the RS simulation are classified into the main rolling texture components of copper texture {90°, 30°, 45°}, brass texture {35°, 45°, 0°/90°} or S texture {55°, 35°, 65°} if their misorientations to the main components are not higher than 5°. The elastic energy of the orientations in the main texture components is calculated according to Equation (5). Figure 5 shows the average elastic energy of orientations. The average elastic energy of cube orientation indicated in Figure 2e is also calculated in a similar manner. Notably, the orientations in different texture components indicate different levels of elastic energy under the same simulation conditions. Brass texture demonstrates much a higher elastic energy in comparison with those of copper, cube and S textures (Figure 5).

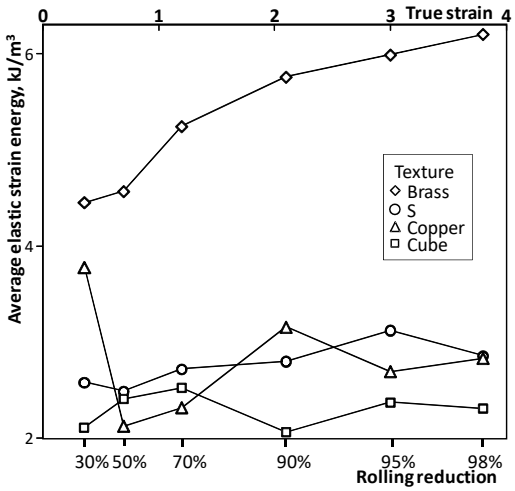

Figure 5. Average elastic energy of grains induced by intergranular mechanical interactions in different texture components during rolling simulation by the RS model (α_{12} = 0.72, α_{23} = α_{31} = 0 and α_{22} = 0.04 for brass, S and copper textures; and α_{12} = 0.8, α_{23} = 1 and α_{31} = α_{22} = 0 for cube texture).

Normally, the stored energy of deformed aluminum approximates 2000 kJ/m^3 and reaches 300 kJ/m^3 if the deformed aluminum is recovered [14]. In comparison, the elastic strain energy (Figure 5) is much lower. However, the level of elastic strain energy in differently oriented deformation grains can still exhibit certain effects during the following thermal treatment. Notably, a cube texture commonly forms after the recrystallization annealing of cold-rolled aluminum sheets. In general, specific cube-oriented nuclei should first be observed, wherein rapid growth will induce the formation of the cube texture [19]. The RS model indicates that the intergranular RSs during rolling ensure (Figure 2d) that a cube-oriented structure can obtain stability and survive rolling deformation. Studies have reported that the cube structure contains low dislocation density and can be preferentially transformed into recrystallization nuclei if it exists in the deformation matrix [20]. The RS model also indicates that very limited elastic strain energy can remain around the cube structure (Figure 5). This condition increases the structure stability and the potential to become nuclei during recovery before primary recrystallization.

Two commercial-purity aluminum samples (99.9% Al) identified as Q and W were cut, possessing a final thickness of 6.9 mm. The samples were cold-rolled down to a 95% reduction. Recovery annealing was conducted at 240 °C for 10 min in a salt bath, but no recrystallization occurred. Figure 6 shows the sheet textures before and after recovery annealing in the form of ODF fiber analysis. Both samples obtained copper {112}<111>, S {123}<634> and brass {110}<112> textures in β-fibers before annealing (Figure 6a,c), in which a copper texture and brass texture were strongly observed in samples Q and W, respectively. Annealing caused no change in the texture type but affected ODF densities to a certain extent, in which the copper texture was strengthened and the brass texture was weakened in both samples. The reduced density peaks of brass texture moved along α-fiber slightly toward the Goss {110}<001> orientation (Figure 6b,d). The phenomena should be related to the elastic strain energy after rolling (Figure 5).

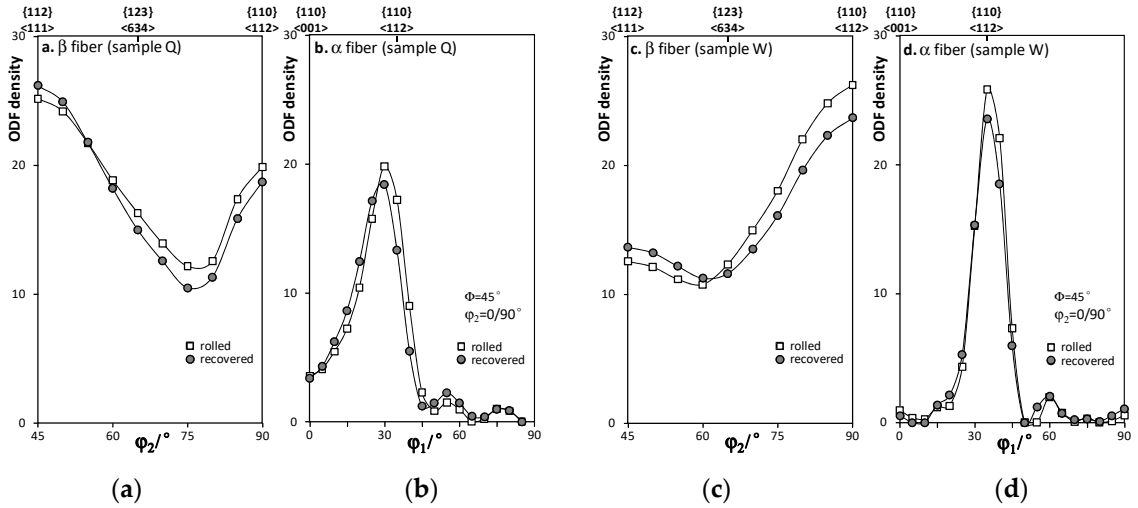

Figure 6. ODF fiber analysis of texture in 95% rolled and recovered aluminum sheets. (**a**) β-Fiber of sample Q; (**b**) α-fiber of sample Q; (**c**) β-fiber of sample W; (**d**) α-fiber of sample W.

Multiple slips caused no high accumulation of RSs during the formation of copper texture (Figure 5), which became strong and sharp after recovery, whereas the stored energy and lattice tortuousness were reduced. However, under the same simulation conditions of the RS model, high RSs accumulated during the formation of brass texture (Figure 5), to which many orientations will move along the α-fiber during rolling [16–18]. Notably, brass texture is not as stable as copper texture. The backward movement of brass texture along α-fiber (Figure 6b,d) during recovery can release a portion of the elastic strain energy accumulated during rolling. According to this condition, the orientation-dependent elastic strain energy, which will influence recovery, may expand its effect into the following recrystallization, including nucleation and grain growth.

6. Summary

The RS model based on the combination of external and intergranular interaction stresses during the plastic deformation of polycrystalline metals is improved by integrating the normal RS σ_{22} in the TD of rolling sheets into the model. Thus, all the possible RSs are effective and can be adjusted separately to reach the necessary stress and strain equilibria in a reasonable manner. Furthermore, the work hardening effect represented by an effective dislocation distance is connected with the engineering strength level of the metals. The model can accurately predict the brass, copper and S textures in aluminum rolling sheets both in terms of orientation positions of the textures and their peak densities. Cube orientation, which is very important for the formation of recrystallization cube texture in aluminum sheets, can reach stability during rolling under the effect of intergranular RSs, especially σ_{22}, of which the stability could not be predicted by other deformation models. RS σ_{12} is commonly accumulated to high levels and jointly determines the selection of penetrating slips and orientation evolution together with external stress, whereas RS σ_{23} and σ_{31} hardly accumulate and can only promote the activation of nonpenetrating slips around the boundary areas and random texture formation. RSs will yield certain orientation-dependent elastic strain energy around the deformation grains, which could not be predicted by other models. The elastic energy is much lower than the stored energy but can lead to different grain stabilities after deformation and may extend its influence during subsequent thermal treatment, e.g., recovery and recrystallization.

Funding: This research was funded by the National Natural Science Foundation of China, grant No. 51571024.

Conflicts of Interest: The authors declare no conflict of interest.

References

1. Taylor, G.I. Plastic strain in metals. *J. Inst. Met.* **1938**, *62*, 307–324.
2. Lebensohn, R.A.; Tomé, C.N.; Castañeda, P.P. Self-consistent modelling of the mechanical behaviour of viscoplastic polycrystals incorporating intragranular field fluctuations. *Philoso. Mag.* **2007**, *87*, 4287–4322. [CrossRef]
3. Van Houtte, P.; Li, S.; Seefeldt, M.; Delannay, L. Deformation texture prediction: From the Taylor model to the advanced lamel model. *Int. J. Plast.* **2005**, *21*, 589–624. [CrossRef]
4. Mu, S.; Tang, F.; Gottstein, G. A cluster-type grain interaction deformation texture model accounting for twinning-induced texture and strain-hardening evolution: Application to magnesium alloys. *Acta Mater.* **2014**, *68*, 310–324. [CrossRef]
5. Mao, W. On the Taylor principles for plastic deformation of polycrystalline metals. *Front. Mater. Sci.* **2016**, *10*, 335–345. [CrossRef]
6. Chapuis, A.; Liu, Q. Investigating the temperature dependency of plastic deformation in a Mg-3Al-1Zn alloy. *Mater. Sci. Eng. A* **2018**, *725*, 108–118. [CrossRef]
7. Wronski, M.; Kumar, M.A.; Capolungo, L.; McCabe, R.J.; Wierzbanowski, K.; Tomé, C.N. Deformation behavior of CP-titanium: Experiment and crystal plasticity modeling. *Mater. Sci. Eng. A* **2018**, *724*, 289–297. [CrossRef]
8. Chatterjeea, A.; Ghosh, A.; Moitra, A.; Bhaduri, A.K.; Mitra, R.; Chakrabarti, D. Role of hierarchical martensitic microstructure on localized deformation and fracture of 9Cr-1Mo steel under impact loading at different temperatures. *Int. J. Plast.* **2018**, *104*, 104–133. [CrossRef]
9. Chelladurai, I.; Adams, D.; Fullwood, D.T.; Miles, M.P.; Niezgoda, S.; Beyerlein, I.J.; Knezevice, M. Modeling of trans-grain twin transmission in AZ31 via a neighborhood-based viscoplastic self-consistent model. *Int. J. Plast.* **2018**, in press. [CrossRef]
10. Zecevic, M.; Lebensohn, R.A.; McCabe, R.J.; Knezevic, M. Modeling of intragranular misorientation and grain fragmentation in polycrystalline materials using the viscoplastic self-consistent formulation. *Int. J. Plast.* **2018**, *109*, 193–211. [CrossRef]
11. Mao, W. The currently predominant Taylor principles should be disregarded in the study of plastic deformation of metals. *Front. Mater. Sci.* **2018**, *12*, 322–326. [CrossRef]
12. Mao, W.; Yu, Y. Effect of elastic reaction stress on plastic behaviors of grains in polycrystalline aggregate during tensile deformation. *Mater. Sci. Eng. A* **2004**, *367*, 277–281. [CrossRef]
13. Mao, W. Intergranular mechanical equilibrium during the rolling deformation of polycrystalline metals based on Taylor principles. *Mater. Sci. Eng. A* **2016**, *672*, 129–134. [CrossRef]
14. Hornbogen, E.; Warlimont, H. *Metallkunde*, 2nd ed.; Springer: New York, NY, USA, 1991; pp. 100–105.
15. Sachs, G. Zur Ableitung einer Fließbedingdung. *Zeitschrift des Vereines deutscher Ingeniere* **1928**, *72*, 732–736.
16. Mao, W. Rolling texture development in aluminum. *Chin. J. Met. Sci. Tech.* **1991**, *7*, 101–112.
17. Mao, W. Modeling of rolling texture in aluminum. *Mater. Sci. Eng. A* **1998**, *257*, 171–177. [CrossRef]
18. Hirsch, J.; Lücke, K. Mechanism of deformation and development of rolling texture in polycrystalline fcc metals-II. *Acta Metall.* **1998**, *36*, 2883–2904. [CrossRef]
19. Mao, W.; Yang, P. Formation mechanisms of recrystallization textures in aluminum sheets based on theories of oriented nucleation and oriented growth. *Trans. Nonferrous Met. Soc. China* **2014**, *24*, 1635–1644. [CrossRef]
20. Mao, W. Formation of recrystallization cube texture in high purity FCC metal sheets. *J. Mater. Eng. Perf.* **1999**, *8*, 556–560. [CrossRef]